Modeling of beech wood pellet pyrolysis under concentrated solar radiation

Kuo Zeng [a], José Soria [b], Daniel Gauthier [a], Germán Mazza [b], Gilles Flamant [a, *]

[a] Processes Materials and Solar Energy Laboratory, PROMES-CNRS, 7 Rue du Four Solaire, 66120, Odeillo Font Romeu, France
[b] Institute for Research and Development in Process Engineering, Biotechnology and Alternative Energies (PROBIEN, CONICET — UNCo), 1400 Buenos Aires St., 8300, Neuquén, Argentina

ARTICLE INFO

ABSTRACT

A two-dimensional, unsteady CFD (Computational Fluid Dynamics) single particle model was developed and used to simulate the solar pyrolysis process of beech wood pellets (10 mm in diameter and 5 mm in height). Pseudo-stoichiometric coefficients about the mass fraction of primary tar converted by the reaction into gas and secondary tar were determined at different temperatures and heating rates for the first time. The 2D model predictions were successfully validated with tests performed at 600 °C to 2000 °C final temperature, with 10 and 50 °C/s heating rates. The evolution of the final products and mass losses of pyrolyzed biomass are enhanced with temperature and heating rate. Moreover, the higher the temperature and heating rate, the higher the gas yield. This emphasizes the intra-particle tar secondary reaction into gas for pyrolysis of large size sample under high temperature and heating rate.

© 2016 Elsevier Ltd. All rights reserved.

1. Introduction

Sustainable heat and power generation from renewable energy sources such as biomass and solar attract more and more attention owing to the continuous diminution of fossil fuels and the intensifying environmental problems. Between 2010 and 2040 significant developments in renewable energy production are expected in biomass energy (from 45217.4 to 136950.2 PJ) and solar energy (from 184.2 to 55768.2 PJ) [1].

However, the low energy density is the biggest obstacle to the biomass usage. Solar energy utilization is impacted by its diluted, intermittent and unequally distributed features. These drawbacks can be overcome by converting biomass and solar energy into solar fuels. Hybrid solar/biomass endothermic process in which biomass is used as chemical reactants and solar energy as the process heat is a good strategy. Indeed in such a process, concentrated solar radiation is the energy source of high-temperature process heat for biomass pyrolysis reactions [2]. There are three main advantages from this combination [3]: (1) Gas pollutants discharge is avoided. (2) The feedstock calorific value is upgraded. (3) The intermittent

solar energy is chemically stored in the form of solar fuels. In the 1980s, Beatie et al. [4] obtained a maximum gas yield of 31 mmol/g coal from direct solar pyrolysis at flux level of 1 MW/m². Recently, bio-char [5], bio-gas [6–8] and bio-oil [9,10] with potential use were produced through solar pyrolysis process.

Solar pyrolysis is carried out under concentrated solar radiation. Some effort has been expended experimentally and theoretically for the better understanding of the complex mechanisms in biomass pyrolysis under simulated solar radiation in image furnace. The image furnace consists in a xenon lamp (light source) associated to a set of concentrating mirrors, which can be adjusted to the required concentrated radiant flux. Reviewing biomass pyrolysis modeling reveals the comprehensive chemical and physical processes [11]. The theoretical and experimental study of cellulose pellets flash pyrolysis submitted to concentrated radiation validated the simple kinetic pathways derived from "Broido-Shafizadeh" model [12]. The three-parallel reaction scheme just considering char, tar and gas was used for biomass pyrolysis in image furnace [13,14]. Both Eulerian and Lagrangian modeling approaches agreed well with the experimental results obtained with oak pellets' fast pyrolysis in an image furnace. They showed that the liquid yield (approximately 62%) did not change with the heat flux density (from 0.3 to 0.8 MW/m²), whereas the gas and char yields

Nomenclature

Latin letters

A	Pre-exponential factor, 1/s
a	Stoichiometric coefficient to gas, —
B	Permeability, m^2
b	Stoichiometric coefficient to secondary tar, —
C_p	Heat capacity, J/kg/K
D	Diffusion coefficient, m^2/s
d_{pore}	Pore diameter, m
E	Activation energy, J/mol
F	Momentum source term, Pa/m
e	Emissivity, —
g	Gravity, m/s^2
k	Reaction rate constant, 1/s
L	Length, m
M	Molar mass, kg/mol
m	Mass, kg
P	Pressure, Pa
Q	Heat generation, W/m^3
R	Radius, m
R_g	Ideal gas constant, J/mol/K
x	Cylindrical coordinate (heating direction), m
r	Cylindrical coordinate (radius direction), m
S	Source term, kg/m^3/s
T	Temperature, K
t	Time, s
v	Velocity, m/s

Greek letters

Δh	Reaction heat, J/kg
ΔT	Temperature difference, K
Δt	Time difference, s
ε	Porosity, —
λ	Thermal conductivity, W/m/K
μ	Viscosity, Pa s
ρ	Apparent density, kg/m^3
$\widehat{\rho}$	Intrinsic density, kg/m^3
η	Pyrolysis degree, —

Subscripts

S	Solid
i	Component (w, c, is)
Ar	Argon
c	Char
cond	Conductive
g	Gas
is	Intermediate solid
r	Radial direction
rad	Radiative
t1	Primary tar
t2	Secondary tar
V	Volatiles (g, t1, t2)
w	Wood
x	X direction

increased and decreased, respectively [13]. A single particle model predicting the evolution of products and mass losses of biomass pellets submitted to concentrated radiation was developed [14]. In such image furnaces, condensable vapors and gases released from the biomass samples were quenched immediately. Tar secondary reactions were not considered in all above models. Actually, primary pyrolysis products (vapors and gases) must diffuse out of the pellets through the hot temperature char layer. Thus, chemical processes of biomass pyrolysis may be described through a primary stage and a secondary stage [15—17]. Chan et al. [15] developed a mathematical wood pyrolysis model inclusive of water release, tar cracking and char deposition chemical reactions, which can be used for predicting the ultimate product distribution and can aid in process optimization to either maximize or minimize the tar production. A coupled transport and reaction model of biomass pyrolysis including shrinkage has been developed by Di Blasi et al. [16]. The experimental and simulation results of wooden particles subjected to an assigned external radiation reveal that the tar secondary reaction is enhanced with the heat flux. Grønli et al. presented a competitive reaction model including a secondary tar cracking step, which can be used to predict the effects of heat flux on the product distribution for biomass pyrolysis [17]. Recently, a few researchers developed models to study the effect of process parameters, such as radiant heat flux, on the product distribution from biomass pyrolysis [18,19]. However, there is no modeling investigation validated experimentally by biomass pyrolysis using a real solar furnace. Up to now, the pyrolysis parameters' influence on product distribution in real solar reactor was only reported in our previous studies [6—8]. Both temperature and heating rate can be used to influence and determine the proportions of the main products of solar pyrolysis process and their characteristics.

Most previous models were developed on the basis of the experimental results obtained by pellet pyrolysis under low heating rates [13,15—19]. Actually, solar pyrolysis has the advantage of high temperature and fast heating rate. The reaction rate constant depends on the heating rate [20]. So a kinetics selection based on fast heating rate experimental tests has been done for modeling solar pyrolysis under severe conditions (heating rate up to 450 °C/s and temperature up to 2000 °C). For wood pellet exposed to concentrated solar radiation, a char layer close to the exposed surface is formed. The pyrolyzing zone propagates into the pellet interior with heat transport. The secondary tar reaction may occur when the interior primary tar flows out through the high temperature char layer. Therefore, it is essential to take into account intra-particle heat and mass transfer and tar secondary reaction in solar pyrolysis model.

Kinetic parameters of biomass pyrolysis depend on the heating rate and final temperature reached [21—23]. They play an important role in determining the pyrolysis product distribution [24—26]. The understanding of kinetics of pyrolysis process and accurate prediction of pyrolysis rates are very much important for optimal design of pyrolysis reactor. Some kinetic models have already been developed to study how these two parameters affecting the pyrolysis chemical and physical processes in conventional reactors [27,28]. For this reason, a two-dimensional, unsteady single particle model, was developed and used to simulate the solar pyrolysis of beech wood pellets under various temperatures and heating rates. The model describes the transport phenomena along with the kinetics that take place in a biomass pellet during solar pyrolysis. The formulated model should allow a deeper understanding of the behavior of intra-particle heat/mass transfer processes and of the tar secondary reactions effects.

2. Experiment

Solar pyrolysis experiments were performed in a 1.5 kW vertical-axis solar furnace, as described in Ref. [6] (Fig. 1). In such a solar furnace, a sensor detects the sun's location and permits its tracking along daytime. The maximum power and flux density of this solar furnace are approximately 1.5 kW and 12,000 kW/m^2, respectively, for 1000 W/m^2 Direct Normal Irradiance (DNI). A shutter composed of moving parallel carbon composite blades modulates the reflected solar beam and thus the incident radiation, and therefore the concentrated flux impinging the sample (biomass pellet set in a crucible) and finally the sample temperature. A transparent Pyrex balloon reactor with 185 mm diameter (6 L volume), set at the focus of the solar furnace, is swept with an argon flow controlled by a mass flowmeter (Bronkhorst, EL-FLOW®). A portable infrared gas analyzer (3100 SYNGAS) equipped with an oxygen detector is used to monitor the gas emission as a function of time and the oxygen concentration during the sweeping process. The sweep gas is mostly used to keep the reactor wall clean. The sample surface temperature is measured by a "solar-blind" optical pyrometer (KLEIBER monochromatic operating at 5.2 μm, in a H$_2$O absorption band, in order to eliminate parasitic reflected solar radiation on the sample surface) through a fluorine window (transparent at this wavelength). The target heating rate and final temperature are set on a PID controller, which controls the shutter opening based on the measured sample temperature.

Beech wood pellets approximately 0.3 g with 10 mm diameter and 5 mm height were placed in a graphite crucible, as indicated in Fig. 2. The beech wood sawdust was dried in an oven at 105 °C for 24 h before compaction. The ultimate and proximate analysis of pellets can be determined with the description in Ref. [6]. The Solar pyrolysis experiments were carried out under the following conditions: pressure 0.44 bar, argon flow rate 6NL/min, heating rate 10 and 50 °C/s, to the final temperature ranging from 600 to 2000 °C. The final temperatures were set constant for 5 min. Following pyrolysis, the pyrolysis products (the condensable vapors and incondensable gases) firstly pass through a liquid collection system. Then permanent gases are aspirated by the vacuum pump and collected in a sampling bag. Finally, compositions (Ar, H$_2$, CO, CO$_2$, CH$_4$, and C$_2$H$_6$) were analyzed by gas chromatography (SRA Instruments MicroGC 3000). After injection of 1–10 μL of gas, columns A and B separate the sample into component gas in less than 180 s. Then the micro thermal conductivity detector (TCD) detects the gas compositions with a 5 ms response time. The solid left in the crucible after experiment was considered as "char". Gas collected in the sampling gas was supposed to be "gas". The liquid product trapped by dry ice condensation train was taken as "oil". The char mass was weighed at the end of each experiment. The gas yield was calculated based on the Ideal Gas Law and gas compositions were determined by micro-gas chromatography. The liquid yield was determined by mass balance.

3. Numerical model

3.1. Proposed kinetic scheme

The modified wood pyrolysis kinetic scheme (Fig. 3) employed in this study is based on the models proposed by Park et al. [29] and Suuberg et al. [30]. In this mechanism, wood is assumed to first break into three primary fractions (gas, primary tar and intermediate solid) by three competing endothermic reactions [29]. Then, if the primary tar residence time inside the pellet is long enough, intra-particle secondary reactions may occur and they decompose the primary tar into gas, char and secondary tar. Additionally, intermediate solid is converted into char by an exothermic reaction [30]. According to the adopted mechanism, the final yield of tar and gas by solar pyrolysis may result from primary pyrolysis and/or secondary pyrolysis within the pellet [31]. The kinetic parameters and heats of pyrolysis reactions for the modified model were obtained from literature; they are listed in Table 1. Reaction rates were assumed to follow Arrhenius law (Eq. (1)). Arrhenius' expression gives the dependence of the rate constant k_i of a chemical reaction with the absolute temperature T, where A_i is the pre-exponential factor (or simply the pre-factor), E_i is the activation energy, and R is the universal gas constant.
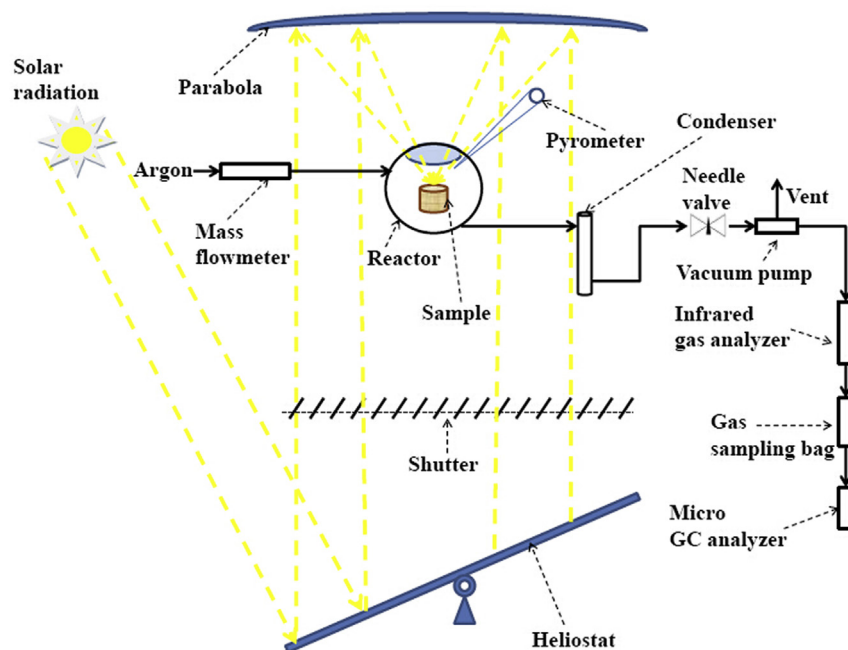

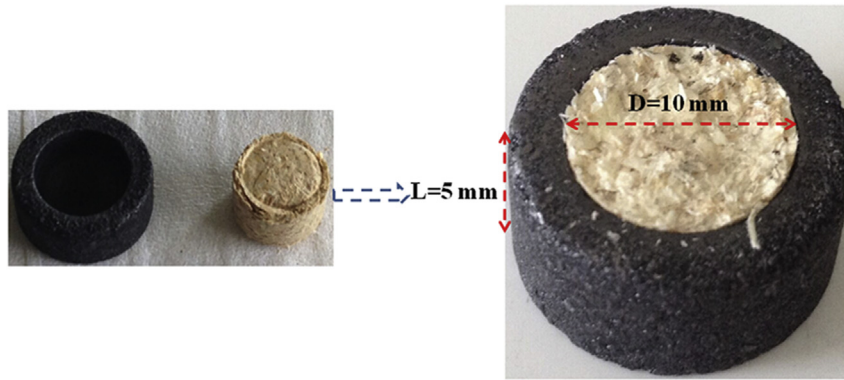**Fig. 1.** Schematic of the solar pyrolysis experimental setup.

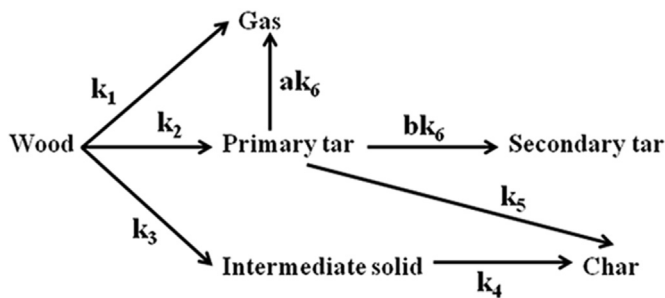**Fig. 2.** Beech wood pellet placed in a graphite crucible.

Fig. 3. Modified wood pyrolysis model.

components degrade differently through various reactions depending on the temperature, to yield different product spectra [36]. Then the use of first-order Arrhenius type reactions is a simplified assumption that does not take into account all complex pyrolysis reactions. Tar is a complex mixture of condensable hydrocarbons, which includes single to 5-ring, other oxygen-containing and complex polycyclic aromatic hydrocarbons [37]. Levoglucosan and phenol are known as the major compounds of primary and secondary tars, respectively [38]. Therefore, primary and secondary tars are assumed to be levoglucosan and phenol for model simplification. Besides, several reactions with different intermediate products are lumped into limited reactions and prod-

Table 1
Kinetic parameters and reaction heat.

Reaction i	A_i (1/s)	E_i (J/kmol)	Δh_i (kJ/kg)	Reference
1 (Wood → gas)	4.38×10^9	152,700	80	[29]
2 (Wood → primary tar)	1.08×10^{10}	148,000	80	[29]
3 (Wood → intermediate solid)	3.27×10^6	111,700	80	[32]
4 (Intermediate solid → char)	1.38×10^{10}	161,000	−300	[29]
5 (Primary tar → char)	1.0×10^5	108,000	−42	[29]
6 (Primary tar → gas)	3.30×10^{11}	141,000	−42	[30]
(Primary tar → secondary tar)				

$$k_i = A_i \exp(-E_i/RT) \tag{1}$$

The values of the pseudo-stoichiometric coefficients a and b (Fig. 3) are assumed to represent the mass fraction of primary tar converted by the secondary reaction to gas and secondary tar, respectively [31]. Chan et al. have assumed that coefficients a and b are adjustable, however, the detailed values are not presented [15]. These coefficients a and b are considered as 0.5 and 0.5, and they are supposed to be constant in Ref. [31]. a and b were determined experimentally as 0.65 and 0.35 for wood slow pyrolysis [33]. It was reported that increasing the temperature and heating rate led to lower tar yield and higher gas yield resulting from tar secondary reactions [6,34]. This implies that the stoichiometric coefficient a (the mass fraction of primary tar converted to gas by the reaction) is generally higher at higher temperature and heating rate. For this reason, stoichiometric coefficients a and b indicated in Table 2 are assumed to depend on the temperature and heating rate for the model formulation, based on the preliminary experimental results that are not used for the model validation.

Woody biomass typically contains about 40−47 wt% cellulose, 25−35 wt% hemicellulose, and about 16−31 wt% lignin [35]. These

ucts for simplification. With this simplified model, the evolution of pyrolysis lump products, together with heat and mass transfers, can be interpreted.

3.2. Main assumptions

The main assumptions of this mathematic model are listed hereafter:

(1) The beech wood pellet is described by a 2D axi-symmetrical computational domain.
(2) The beech wood pellet is homogeneous with isotropic particle structure.
(3) The temperature is the same for all phases present in the solid particle because of the local thermal equilibrium assumed in the particle domain.
(4) Gas, primary and secondary tars are in gaseous phase, where they obey ideal gas law.
(5) Dry beech wood pellet is considered; hence moisture evaporation stage is not modeled.
(6) Wood shrinkage is not considered.
(7) There is no extra-particle tar secondary reaction.

Table 2
Stoichiometric coefficients a and b used in the model.

		Heating rate intervals (°C/s)	
		Slow	Fast
Temperature intervals (°C)	Low (≤600)	$a = 0.18$; $b = 0.82$	$a = 0.18$; $b = 0.82$
	Intermediate (600−1200)	$a = 0.43$; $b = 0.57$	$a = 0.5$; $b = 0.5$
	High (1200−2000)	$a = 0.5$; $b = 0.5$	$a = 0.7$; $b = 0.3$

3.3. Governing equations

3.3.1. Mass and momentum balances

The solid mass conservation equations are formulated based on the apparent density which is related to intrinsic density according to Eq. (2). However, the intrinsic densities are used for the volatile species in all of the equations.

$$\rho_{s,i} = (1 - \varepsilon)\widehat{\rho}_{s,i} \tag{2}$$

The wood mass balance is given in Eq. (3):

$$\frac{\partial \rho_w}{\partial t} = -(k_1 + k_2 + k_3)\rho_w \tag{3}$$

The intermediate solid mass conservation equation considers its production from biomass conversion and its consumption to produce char, as well as the unsteady term, given in Eq. (4).

$$\frac{\partial \rho_{is}}{\partial t} = k_3 \rho_w - k_4 \rho_{is} \tag{4}$$

In a similar way, the char instantaneous mass balance is expressed as Eq. (5).

$$\frac{\partial \rho_c}{\partial t} = k_4 \rho_{is} + \varepsilon k_5 \rho_{t1} \tag{5}$$

The mass balance for argon, gas, primary tar and secondary tar are expressed by the two-dimensional cylindrical coordinate partial differential equation system shown in Eqs. (6)−(9).

$$\frac{\partial(\varepsilon\rho_{Ar})}{\partial t} + \frac{\partial}{\partial x}\left(\rho_{Ar}v_x - \frac{\partial(D\rho_{Ar})}{\partial x}\right) + \frac{1}{r}\frac{\partial}{\partial r}\left(r\rho_{Ar}v_r - r\frac{\partial(D\rho_{Ar})}{\partial r}\right) = 0 \tag{6}$$

$$\frac{\partial\left(\varepsilon\rho_g\right)}{\partial t} + \frac{\partial}{\partial x}\left(\rho_g v_x - \frac{\partial\left(D\rho_g\right)}{\partial x}\right) + \frac{1}{r}\frac{\partial}{\partial r}\left(r\rho_g v_r - r\frac{\partial\left(D\rho_g\right)}{\partial r}\right) = S_g \tag{7}$$

$$\frac{\partial(\varepsilon\rho_{t1})}{\partial t} + \frac{\partial}{\partial x}\left(\rho_{t1}v_x - \frac{\partial(D\rho_{t1})}{\partial x}\right) + \frac{1}{r}\frac{\partial}{\partial r}\left(r\rho_{t1}v_r - r\frac{\partial(D\rho_{t1})}{\partial r}\right) = S_{t1} \tag{8}$$

$$\frac{\partial(\varepsilon\rho_{t2})}{\partial t} + \frac{\partial}{\partial x}\left(\rho_{t2}v_x - \frac{\partial(D\rho_{t2})}{\partial x}\right) + \frac{1}{r}\frac{\partial}{\partial r}\left(r\rho_{t2}v_r - r\frac{\partial(D\rho_{t2})}{\partial r}\right) = S_{t2} \tag{9}$$

The source terms for gas, primary tar and secondary tar are given in Eqs. (10)−(12).

$$S_g = k_1\rho_w + \varepsilon a k_6 \rho_{t1} \tag{10}$$

$$S_{t1} = k_2\rho_w - \varepsilon(k_5 + k_6)\rho_{t1} \tag{11}$$

$$S_{t2} = \varepsilon b k_6 \rho_{t1} \tag{12}$$

For 2D axi-symmetrical geometries, the axial and radial momentum conservation equations for gas, tar 1 and tar 2 can be written as Eqs. (13)−(17).

$$\begin{aligned}
&\frac{\partial}{\partial t}(\varepsilon\rho v_x) + \frac{1}{r}\frac{\partial}{\partial x}(r\rho v_x v_x) + \frac{1}{r}\frac{\partial}{\partial r}(r\rho v_r v_x) \\
&= -\frac{\partial p}{\partial x} + \frac{1}{r}\frac{\partial}{\partial x}\left[r\mu\left(2\frac{\partial v_x}{\partial x} - \frac{2}{3}(\nabla \times \overrightarrow{v})\right)\right] + \frac{1}{r}\frac{\partial}{\partial r}\left[r\mu\left(\frac{\partial v_x}{\partial r} + \frac{\partial v_r}{\partial x}\right)\right. \\
&\quad \times \Big] + F_x
\end{aligned} \tag{13}$$

$$\begin{aligned}
&\frac{\partial}{\partial t}(\varepsilon\rho v_r) + \frac{1}{r}\frac{\partial}{\partial x}(r\rho v_x v_r) + \frac{1}{r}\frac{\partial}{\partial r}(r\rho v_r v_r) \\
&= -\frac{\partial p}{\partial r} + \frac{1}{r}\frac{\partial}{\partial x}\left[r\mu\left(\frac{\partial v_r}{\partial x} + \frac{\partial v_x}{\partial r}\right)\right] + \frac{1}{r}\frac{\partial}{\partial r}\left[r\mu\left(2\frac{\partial v_r}{\partial r} - \frac{2}{3}(\nabla \times \overrightarrow{v})\right)\right. \\
&\quad \times \Big] - 2\mu\frac{v_r}{r^2} + \frac{2}{3}\frac{\mu}{r}(\nabla \times \overrightarrow{v}) + F_r
\end{aligned} \tag{14}$$

$$\nabla \times \overrightarrow{v} = \frac{\partial v_x}{\partial x} + \frac{\partial v_r}{\partial r} + \frac{v_r}{r} \tag{15}$$

$$F_x = -\frac{\mu}{B}v_x \tag{16}$$

$$F_r = -\frac{\mu}{B}v_r \tag{17}$$

The real-time permeability B of pyrolysis wood is interpolated from the value of pure wood and char as expressed in Eq. (19).

$$B = \eta B_c + (1 - \eta)B_w \tag{19}$$

where η is the conversion factor defined as Eq. (20):

$$\eta = 1 - \frac{\rho_w + \rho_{is}}{\widehat{\rho}_w} \tag{20}$$

The real-time porosity ε can be expressed as Eq. (18).

$$\frac{1 - \varepsilon}{1 - \varepsilon_{w,0}} = \frac{\rho_w + \rho_{is} + \rho_c}{\widehat{\rho}_w} \tag{18}$$

3.3.2. Energy balance

The energy conservation (Eq. (21)) considers the unsteady term, convection and conductive heat transfer and the reaction heats.

$$\left(\rho_w C_{p,w} + \rho_{is} C_{p,is} + \rho_c C_{p,c} + \rho_{t1} C_{p,t1} + \rho_{t2} C_{p,t2} + \rho_g C_{p,g}\right) \frac{\partial(T)}{\partial t}$$
$$+ \frac{\partial\left(\rho_g C_{p,g} v_x T\right)}{\partial x} + \frac{\partial\left(r \rho_g C_{p,g} v_r T\right)}{r \partial r}$$
$$= \frac{\partial}{\partial x}\left(\lambda_{eff(x)} \frac{\partial T}{\partial x}\right) + \frac{\partial}{r \partial r}\left(r \lambda_{eff(r)} \frac{\partial T}{\partial r}\right) + Q$$

$$(21)$$

where Q is the heat source, given in Eq. (22):

$$Q = -(k_1 \Delta h_1 + k_2 \Delta h_2 + k_3 \Delta h_3)\rho_w - k_4 \Delta h_4 \rho_{is} - \varepsilon(k_5 \Delta h_5 + k_6 \Delta h_6)\rho_{t1} \qquad (22)$$

The pellet thermal conductivity is calculated as a linear function of the wood and char conductivities [14] as shown in Eq. (23). The radiant contribution is calculated based on Eq. (24) [39]. The properties of beech wood and char used for the modeling are given in Table 3.

$$\lambda_{cond} = (1 - \eta)\lambda_w + \eta \lambda_c \qquad (23)$$

$$\lambda_{rad} = 16\sigma T^3 e d_{pore} / 3 \qquad (24)$$

Then the pellet effective thermal conductivity can be expressed by the function of intrinsic and radiative conductivities given in Eq. (25). Table 3 shows the thermo-physical data used in the model.

$$\lambda_{eff} = (1 - \varepsilon)\lambda_{cond} + \varepsilon(\lambda_{rad} + \lambda_v) \qquad (25)$$

3.4. Boundary and initial conditions

Fig. 4a schemes the beech wood pellet top being irradiated in a transparent Pyrex reactor. The sidewall and bottom are insulated by the crucible and by graphite foam. Due to symmetry, only half of the pellet is shown in Fig. 4b.
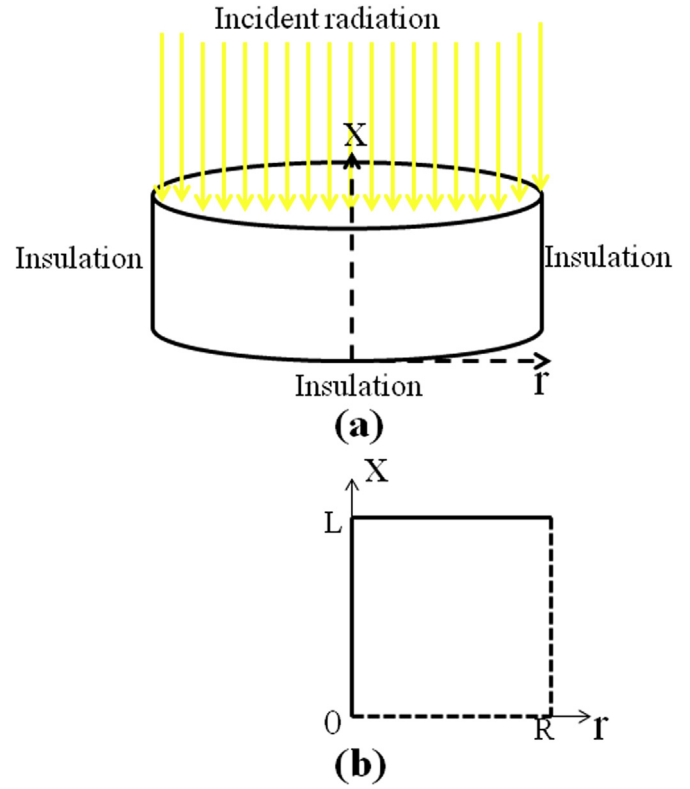

Fig. 4. (a) Pellet boundary conditions; (b) Axi-symmetrical coordinate.

(1) For the irradiated top surface (x = L), the thermal boundary condition is established as the temperature measured during the experiment, as given in Eq. (26).

$$T(L, r, t) = T_{exp}(t) \qquad (26)$$

Table 3
Thermo-physical data used in the model.

Property	Value	Ref.
Radius	$R = 5 \times 10^{-3}$, m	Measured
Length	$L = 5 \times 10^{-3}$, m	Measured
Intrinsic pellet density	$\hat{\rho}_w = 764$, kg/m^3	Measured
Initial pellet porosity	$\varepsilon_{w,0} = 0.365$	Measured
Wood permeability	$B_w = 7.25 \times 10^{-13}$, m^2	[40]
Pore diameter	$d_{pore} = 0.00005$, m	[17]
Intrinsic char density	$\hat{\rho}_c = 2000$, kg/m^3	[40]
Char permeability	$B_c = 10^{-11}$, m^2	[40]
Intrinsic gas density	$\hat{\rho}_g = 1125$, kg/m^3	[40]
Intrinsic wood thermal conductivity	$\lambda_w = 0.291 + 0.000836 \times 0.33T$, W/mK	[41]
Intrinsic char thermal conductivity	$\lambda_c = 1.47 + 0.0011T$, W/mK	[39]
Intrinsic volatile thermal conductivity	$\lambda_V = 0.0258$, W/mK	[17]
Wood specific heat capacity	$C_{p,w} = 2300 - 1500exp(-0.0055T)$,	[40]
Intermediate solid specific heat capacity	$C_{p,is} = 2300 - 1500exp(-0.0055T)$	[40]
Char specific heat capacity	$C_{p,c} = 1430 + 0.355T - 7.3210T^{-2}$	[40]
Primary tar specific heat capacity	$C_{p,t1} = -100 + 4.4T - 1.57 \times 10^{-3}T^2$	[17]
Secondary tar specific heat capacity	$C_{p,t2} = -100 + 4.4T - 1.57 \times 10^{-3}T^2$	[17]
Gas specific heat capacity	$C_{p,g} = 770 + 0.629T - 1.91 \times 10^{-4}T^2$	[17]
Diffusion coefficient	$D = 1.0 \times 10^{-6}$, m^2/s	[15]
Viscosity	$\mu = 3.0 \times 10^{-5}$, Pa s	[33]
Atmosphere pressure	$P_0 = 0.083$ Mpa	Measured
Stefan Boltzmann constant	$\sigma = 5.67 \times 10^{-8}$, W/m^{2}K^4	–
Universal gas constant	$R = 8.314$, J/molK	–
Emissivity	$e = 0.95$	[42]

$$\rho_{Ar}(L, r, t) = \rho_{Ar,bulk} \tag{27}$$

$$\rho_V(L, r, t) = \rho_{V,bulk}(V = g, t1, t2) = 0 \tag{28}$$

$$P = P_0 \quad \text{(pressure outlet)} \tag{29}$$

(2) For the adiabatic sidewalls (r = R) and bottom surface (x = 0)

$$\left.\frac{\partial T}{\partial r}\right|_{r=R} = 0 \tag{30}$$

$$\left.\frac{\partial \rho_V}{\partial r}\right|_{r=R} = 0 \tag{31}$$

$$v = 0 \quad (no-slip\ condition) \tag{32}$$

$$\left.\frac{\partial T}{\partial x}\right|_{x=0} = 0 \tag{33}$$

$$\left.\frac{\partial \rho_V}{\partial x}\right|_{x=L} = 0 \tag{34}$$

$$v = 0 \quad (no-slip\ condition) \tag{35}$$

(3) For the cylindrical pellet center (r = 0), symmetry condition is adopted

$$\left.\frac{\partial T}{\partial r}\right|_{r=0} = 0 \tag{36}$$

$$\left.\frac{\partial \rho_V}{\partial r}\right|_{r=0} = 0 \tag{37}$$

$$\left.\frac{\partial v}{\partial r}\right|_{r=0} = 0 \tag{38}$$

The particle surface is assumed to be initially at 473 K, as measured experimentally.

3.5. Numerical solution

The momentum equation, the species mass conservation equations and the heat transfer equation in the porous particle are solved in a 2-D scheme with the CFD software FLUENT 14.0, using the finite volume discretization method. User-defined functions (UDFs) are programmed in C++ language and complemented to the FLUENT code. UDFs mass sources for gas phases (gas, primary tar and secondary tar) and energy sources for pyrolysis reactions are programmed, as well as the mass source terms for the solids. Moreover, the pellet porosity, effective thermal conductivity and permeability are also programmed.

The "pressure-based method" is used to solve the momentum equation. Pressure-velocity coupling algorithm is used by FLUENT to derive equations for the pressure from the momentum equations and the continuity equation. In this work, the "coupled" algorithm is adopted based on its robustness and efficiency. Additionally, all scalars are discretized by a second order discretization scheme for obtaining more accurate results, with the residuals set at 10^{-6}. Finally, unsteady simulations were carried out with a step size of 0.005 s and 30 iterations per time step.

4. Results and discussion

4.1. Influence of temperature and heating rate on the product distribution

The model was validated against experimental data obtained from solar pyrolysis experiments under two different heating rates: 10 (slow) and 50 °C/s (fast) and five final temperatures: 600, 900, 1200, 1600 and 2000 °C. Figs. 5–7 show the total yields of gas, char and liquid (tar) at these different temperatures and heating rates, respectively. CFD points were obtained by simulation. EXP points are experimental results. Then, the points are real experimental values whereas the lines are only indications of variation trend. As shown in Fig. 5, the gas product yield generally increases with the temperature and heating rate. The gas yield increase is probably due the enhanced tar intra-particle secondary reactions at higher temperatures and heating rates [6]. The model predicts well the experimental gas yields at slow and fast heating rates. The predicted trends of char yield evolution with temperature and heating rate are the same as the experimental ones (Fig. 6). Higher temperature and higher heating rate lead to lower char yield [7]. However, the simulation overestimates experimental results for char yield. This discrepancy may be mainly due to the ignored heterogeneous reactions between char and tar, because of the lack of kinetic data for such reactions, in part because of other parameters uncertainty. Calculated data of liquid yields fit excellently experimental data at both heating rates, as presented in Fig. 7, which shows that the liquid yield decreases with the heating rate. The heating rate increase has two opposite effects on the liquid yield production: (1) The tar intra-particle residence time decreases, and then tar may escape the pellet without reacting; (2) the tar temperature increases faster and quickly decomposes into gas, secondary tar and char. Results may indicate that, with the used size of pellet, the latter effect may be more significant than the first one, enhancing tar decomposition within the pellet before it leaves the pellet surface.

The model was validated with solar pyrolysis data at different temperatures with various heating rates. So it can be used to interpret the weight loss history and gas evolution.
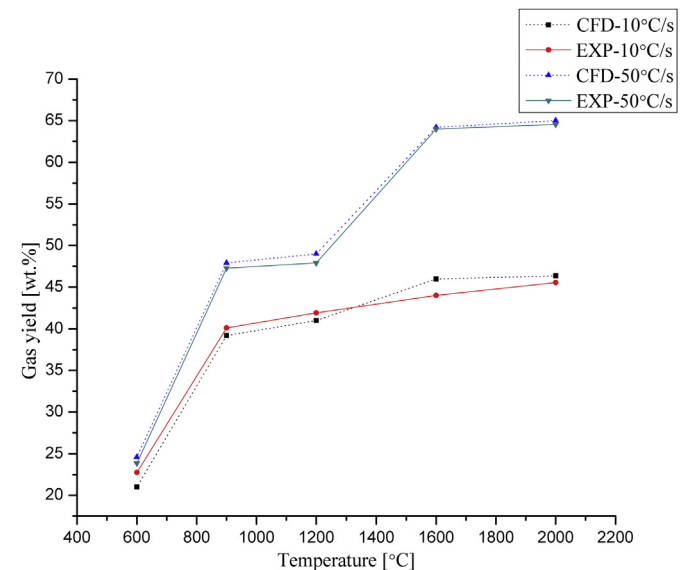

Fig. 5. Gas yield: comparison between the CFD model prediction values and experimental results.
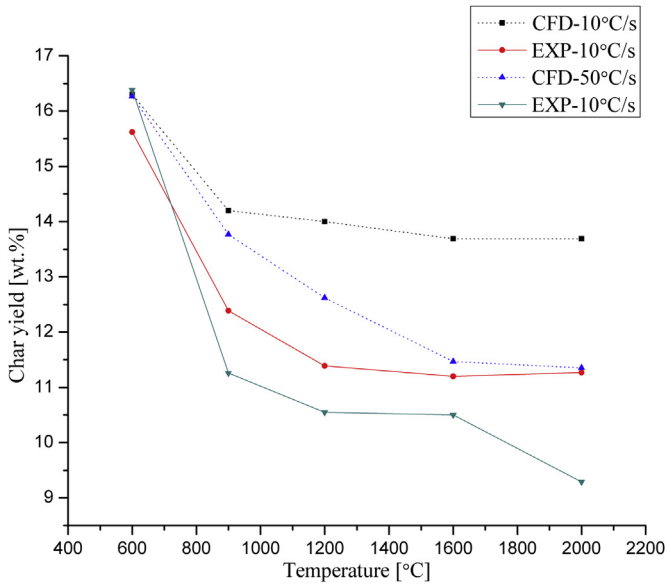
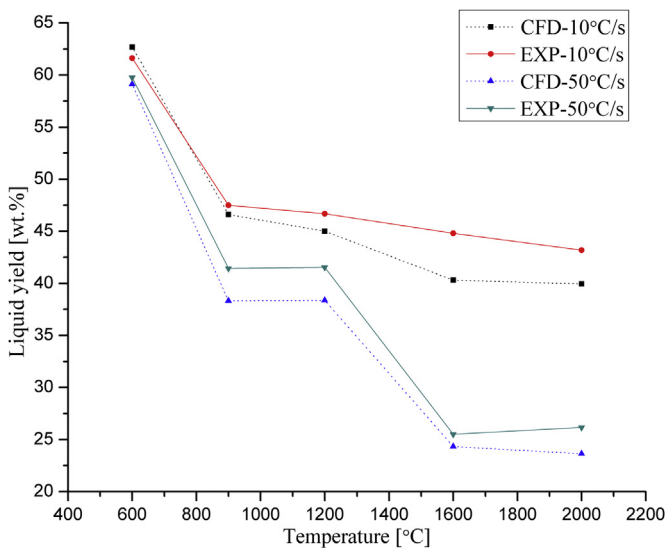**Fig. 6.** Char yield: comparison between the CFD model prediction values and experimental results.

Fig. 7. Liquid (tar) yield: comparison between the CFD model prediction values and experimental results.

4.2. Influence of temperature and heating rate on the weight loss history

The wood density was determined according to the mass conservation Eq. (3) by UDF code. The wood density decreases with time, thus indicating a weight loss. Fig. 8 shows the weight loss history of the pyrolyzed wood under different final temperatures (900−2000 °C) with different heating rates (10 and 50 °C/s). It is clearly seen that with fast heating rate (50 °C/s) sample heating continues until about 10 s when the active decomposition of the sample starts, whatever the final temperature. Oppositely, the sample decomposition begins only at about 30s with slow heating rate (10 °C/s). This implies that the biomass conversion rate at the process onset does not significantly depend on the final temperature, which was also observed by Okekunle et al. [43]. Fast heating rate reduces the time required for the sample to overpass 250 °C,
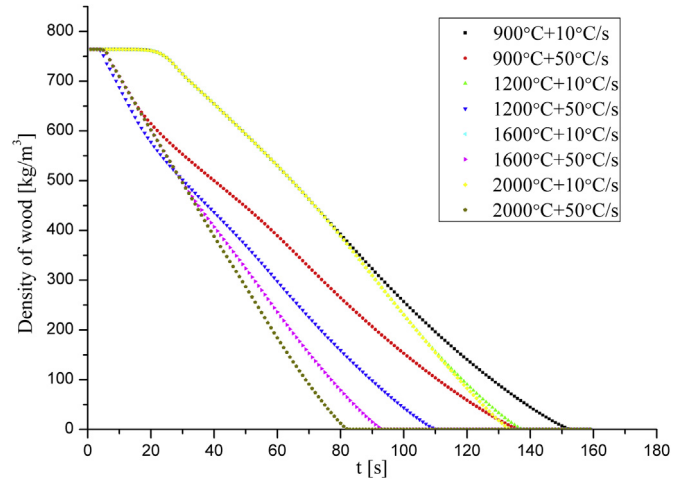

Fig. 8. Weight loss evolution of the pyrolyzed wood under different temperatures and heating rates.

where primary pyrolysis occurs [44]. With a heating rate value of 50 °C/s, the weight loss profile begins to be steeper and steeper when the final temperature increases from 900 to 2000 °C. This may come from the increase of heat transfer rate in the pellet with the final temperature, thereby accelerating the pyrolysis reaction. The longest reaction time is about 150s when the final temperature is 900 °C with heating rate 10 °C/s, and it decreases to about 80 s at the highest temperature and heating rate.

4.3. Influence of temperature and heating rate on gases evolution

Fig. 9 plots the gas release flow rate at different reactor temperatures and heating rates. The figure shows that the maximum values of gas release increase with temperature. This comes from the intra-particle tar secondary reactions that are enhanced at higher temperatures, thereby resulting in drastic increase in the rate of gas release with time. Besides, the gas release rate peaks appear earlier at fast heating rate (50 °C/s) than at slow heating rate (10 °C/s). The gas release rate profiles at fast heating rate (50 °C/s) display two peaks. At low temperature, CO and CO_2 (and water vapor) evolution is mainly due to extractives, hemicellulose, and cellulose degradation, leading to gas and char formation [11]. As the
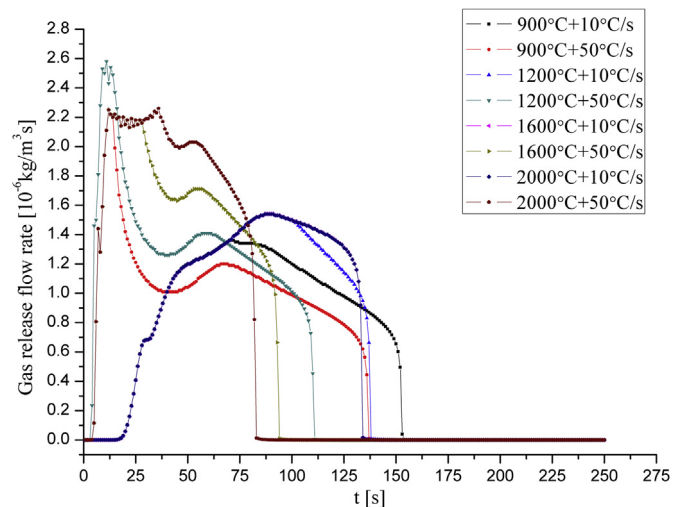

Fig. 9. Gas release flow rate of the pyrolyzed wood under different temperatures and heating rates.

temperature increases, the secondary reaction of tar (mostly from high temperature cellulose degradation) mainly produces CO and H_2 [45]. Then the first peak composed primarily of CO_2, CH_4 and H_2O can be considered to originate from the primary pyrolysis reaction. The second peak may be explained by the tar intra-particle reactions into H_2 and CO. However, there is only one peak for the gas release rate profiles at slow heating rate (10 °C/s). A possible explanation is that longer time is required for the sample to over-pass 500 °C, which is the critical temperature for tar secondary reaction. So the primary reaction will last longer time at slow heating rate, and therefore the secondary and primary reactions may overlap thus producing only one peak, as shown in Fig. 9.

5. Conclusions

Solar pyrolysis characteristics of beech wood under different temperatures and heating rates were investigated theoretically by CFD modeling, and simulation results were compared with experimental data obtained with a 2 kW vertical solar furnace. The 2D unsteady numerical model predictions are in good agreement with the experimental results. The evolution of the final products and mass losses of pyrolyzed biomass are enhanced with temperature and heating rate. Moreover, the higher the temperature and heating rate, the higher the gas yield. This emphasizes the intra-particle tar secondary reaction into gas for pyrolysis of large size sample under high temperature and heating rate. Pseudo-stoichiometric coefficients about the mass fraction of primary tar converted by the reaction to gas and secondary tar were determined at different temperatures and heating rates for the first time.

Acknowledgement

References

[1] REN21, Renewables 2014 Global Status Report, 2014.
[2] N. Piatkowski, C. Wieckert, A.W. Weimer, A. Steinfeld, Solar-driven gasification of carbonaceous feedstock—a review, Energy Environ. Sci. 4 (2011) 73–82.
[3] A. Nzihou, G. Flamant, B. Stanmore, Synthetic fuels from biomass using concentrated solar energy - a review, Energy 42 (2012) 121–131.
[4] W.H. Beattie, R. Berjoan, J.-P. Coutures, High-temperature solar pyrolysis of coal, Sol. Energy 31 (1983) 137–143.
[5] K. Zeng, D.P. Minh, D. Gauthier, E. Weiss-Hortala, A. Nzihou, G. Flamant, The effect of temperature and heating rate on char properties obtained from solar pyrolysis of beech wood, Bioresour. Technol. 182 (2015) 114–119.
[6] K. Zeng, D. Gauthier, R. Li, G. Flamant, Solar pyrolysis of beech wood: effects of pyrolysis parameters on the product distribution and gas product composition, Energy 93 (2015) 1648–1657.
[7] K. Zeng, D. Gauthier, J. Lu, G. Flamant, Parametric study and process optimization for solar pyrolysis of beech wood, Energy Convers. Manag. 106 (2015) 987–998.
[8] R. Li, K. Zeng, J. Soria, G. Mazza, D. Gauthier, R. Rodriguez, G. Flamant, Product distribution from solar pyrolysis of agricultural and forestry biomass residues, Renew. Energy 89 (2016) 27–35.
[9] S. Morales, R. Miranda, D. Bustos, T. Cazares, H. Tran, Solar biomass pyrolysis for the production of bio-fuels and chemical commodities, J. Anal. Appl. Pyrolysis 109 (2014) 65–78.
[10] J.N. Zeaiter, M. Ahmad, D. Rooney, B. Samneh, E. Shammas, Design of an automated solar concentrator for the pyrolysis of scrap rubber, Energy Convers. Manag. 101 (2015) 118–125.
[11] C. Di Blasi, Modeling chemical and physical processes of wood and biomass pyrolysis, Prog. Energy Combust. Sci. 34 (2008) 47–90.
[12] O. Boutin, M. Ferrer, J. Lédé, Flash pyrolysis of cellulose pellets submitted to a concentrated radiation: experiments and modelling, Chem. Eng. Sci. 57 (2002) 15–25.
[13] O. Authier, M. Ferrer, G. Mauviel, A.-E. Khalfi, J. Lédé, Wood Fast pyrolysis: comparison of Lagrangian and Eulerian modeling approaches with experimental measurements, Ind Eng Chem Res. 48 (2009) 4796–4809.
[14] M. Al-Haddad, E. Rendek, J.P. Corriou, G. Mauviel, Biomass fast pyrolysis: experimental analysis and modeling approach, Energy Fuels 24 (2010) 4689–4692.
[15] W.C. Chan, M. Kelbon, B.B. Krieger, Modelling and experimental verification of physical and chemical processes during pyrolysis of a large biomass particle, Fuel 64 (1985) 1505–1513.
[16] C. Di Blasi, Heat, momentum and mass transport through a shrinking biomass particle exposed to thermal radiation, Chem. Eng. Sci. 51 (1996) 1121–1132.
[17] M.G. Grønli, M.C. Melaaen, Mathematical model for wood pyrolysis comparison of experimental measurements with model predictions, Energy Fuels 14 (2000) 791–800.
[18] V. Pozzobon, S. Salvador, J.J. Bézian, M. El-Hafi, Y. Le Maoult, G. Flamant, Radiative pyrolysis of wet wood under intermediate heat flux: experiments and modelling, Fuel Process. Technol. 128 (2014) 319–330.
[19] S.D. Kenarsari, Y. Zheng, Fast pyrolysis of biomass pellets using concentrated solar radiation: a numerical study, J. Sol. Energy Eng. 136 (2014) 041004.
[20] M. Van de Velden, J. Baeyens, A. Brems, B. Janssens, D. Raf, Fundamentals, kinetics and endothermicity of the biomass pyrolysis reaction, Renew. Energy 35 (2010) 232–242.
[21] Y.G. Liang, B. Cheng, Y.B. Si, D.J. Cao, H.Y. Jiang, G.M. Han, X.H. Liu, Thermal decomposition kinetics and characteristics of Spartina alterniflora via thermogravimetric analysis, Renew. Energy 68 (2014) 111–117.
[22] D. Vamvuka, S. Sfakiotakis, Effects of heating rate and water leaching of perennial energy crops on pyrolysis characteristics and kinetics, Renew. Energy 36 (2011) 2433–2439.
[23] H. Haykiri-Acma, S. Yaman, S. Kucukbayrak, Effect of heating rate on the pyrolysis yields of rapeseed, Renew. Energy 31 (2006) 803–810.
[24] Y.K. Park, M.L. Yoo, H.W. Lee, S.H. Park, S.C. Jung, S.S. Park, S.C. Kim, Effects of operation conditions on pyrolysis characteristics of agricultural residues, Renew. Energy 42 (2012) 125–130.
[25] S.H. Beis, Ö. Onay, Ö.M. Koçar, Fixed-bed pyrolysis of safflower seed: influence of pyrolysis parameters on product yields and compositions, Renew. Energy 26 (2002) 21–32.
[26] P.T. Williams, S. Besler, The influence of temperature and heating rate on the slow pyrolysis of biomass, Renew. Energy 31 (1996) 233–250.
[27] R. Sharma, P.N. Sheth, A.M. Gujrathi, Kinetic modeling and simulation: pyrolysis of Jatropha residue de-oiled cake, Renew. Energy 86 (2016) 554–562.
[28] Z. Luo, S. Wang, K. Cen, A model of wood flash pyrolysis in fluidized bed reactor, Renew. Energy 30 (2005) 377–392.
[29] W.C. Park, A.R. Atreya, H. Baum, Experimental and theoretical investigation of heat and mass transfer processes during wood pyrolysis, Combust. Flame 157 (2010) 481–494.
[30] M.E. Suuberg, I. Milosavljevic, V. Oja, Two-regime global kinetics of cellulose pyrolysis: the role of tar evaporation, Sym. Int. Combust. 26 (1996) 1515–1521.
[31] E. Grieco, G. Baldi, Analysis and modeling of wood pyrolysis, Chem. Eng. Sci. 66 (2011) 650–660.
[32] C. Di Blasi, C. Branca, Kinetics of primary product formation from wood pyrolysis, Ind. Eng. Chem. Res. 40 (2001) 5547–5556.
[33] J. Ratte, F. Marias, J. Vaxelaire, P. Bernada, Mathematical modelling of slow pyrolysis of a particle of treated wood waste, J. Hazard. Mater. 170 (2009) 1023–1040.
[34] R. Zanzi, K. Sjostrom, E. Bjornbom, Rapid pyrolysis of agricultural residues at high temperature, Biomass Bioenergy 23 (2002) 357–366.
[35] D. Mohan, C.U. Pittman Jr., P.H. Steele, Pyrolysis of wood/biomass for bio-oil, Energy Fuels 20 (2006) 848–889.
[36] H. Yang, R. Yan, H. Chen, C. Zheng, D.H. Lee, D.T. Liang, In-depth investigation of biomass pyrolysis based on three major components: hemicellulose, cellulose and lignin, Energy Fuels 20 (2006) 383–393.
[37] L. Devi, K.J. Ptasinski, F.J. Janssen, A review of the primary measures for tar elimination in biomass gasification processes, Biomass Bioenergy 24 (2003) 125–140.
[38] P. Morf, P. Hasler, T. Nussbaumer, Mechanisms and kinetics of homogeneous secondary reactions from continuous pyrolysis of wood chips, Fuel 81 (2002) 843–853.
[39] H. Thunman, B. Leckner, Thermal conductivity of wood—models for different stages of combustion, Biomass Bioenergy 23 (2002) 47–54.
[40] J. Blondeau, H. Jeanmart, Biomass pyrolysis at high temperatures: prediction of gaseous species yields from an anisotropic particle, Biomass Bioenergy 41 (2012) 107–121.
[41] T. Harada, T. Hata, S. Ishihara, Thermal constants of wood during the heating process measured with the laser flash method, J. Wood Sci. 44 (1998) 425–431.
[42] B.V. Babu, A.S. Chaurasia, Modeling for pyrolysis of solid particle: kinetics and heat transfer effects, Energy Convers. Manag. 44 (2003) 2251–2275.
[43] P.O. Okekunle, Effect of peak temperature on biomass pyrolysis characteristics in thermally thin regime in a fixed-bed reactor, Math. Theory Model. 5 (2015) 136–146.
[44] D. Neves, H. Thunman, A. Matos, L. Tarelho, A. Gómez-Barea, Characterization and prediction of biomass pyrolysis products, Prog. Energy Combust. Sci. 37 (2011) 611–630.
[45] J. Rath, G. Staudinger, Cracking reactions of tar from pyrolysis of spruce wood, Fuel 80 (2001) 1379–1389.